Chemical Engineering & Processing: Process Intensification 207 (2025) 110077

Contents lists available at ScienceDirect

Chemical Engineering and Processing - Process Intensification

journal homepage: www.elsevier.com/locate/cep

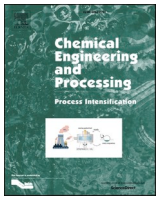

Intensified co-precipitation and ion exchange using an agitated tubular reactor (ATR) for enhanced removal of Cs^{+} and Sr^{2+} ions

Oguzhan Kivan [a,*], Muhammad Yusuf [a,b,c], Rachael Filson-Halliwell [a], Jennifer N. Enemmoh [a], David Harbottle [a], Timothy N. Hunter [a,*]

[a] School of Chemical and Process Engineering, University of Leeds, Leeds, LS2 9JT, UK
[b] Research Centre for Nuclear Material and Radioactive Waste Technology (PRTBNLR), Research Organization for Nuclear Energy (ORTN), National Research and Innovation Agency (BRIN), South Tangerang, 15314, Indonesia
[c] Interdisciplinary Research Center for Industrial Nuclear Energy (IRC-INE), King Fahd University of Petroleum & Minerals (KFUPM), Dhahran, 31261, Kingdom of Saudi Arabia

ARTICLE INFO

Keywords:
Clinoptilolite
Ion exchange
Coagulation
Agitated tubular reactor
Process intensification
Pressure filtration

ABSTRACT

Composite coagulants were synthesised in both a batch system and an agitated tubular reactor (ATR) using natural clinoptilolite with barite ($BaSO_4$) co-precipitation for the intensified simultaneous removal of Cs^{+} and Sr^{2+} ions. Ideal plug-flow characterisation of ATR was initially assessed under 3 and 5 Hz oscillations, showing pseudo plug-flow behaviour at the higher rate. Composite flocs were characterised by SEM and size analysis, while dewaterability was also studied by sedimentation and pressure filtration. Aggregate sizes were smaller, but denser and more monodisperse from the ATR than in batch. Composite flocs also gave measured specific cake resistances $> 10 \times$ smaller than pure $BaSO_4$. The higher metal removal performance was achieved using the ATR for Cs^{+} (95.7%) and Sr^{2+} (99.9%) at 5 Hz oscillation. A further enhancement for Cs^{+} removal was achieved by introducing Ba^{2+} ions into ATR after Na_2SO_4 addition, achieving $>$ 96% Cs^{+} and $>$ 99.9% Sr^{2+} removal. Overall, this study highlights that composite flocs outperform pure $BaSO_4$ in Cs^{+} and Sr^{2+} ion removal while achieving greater dewaterability and filterability. Additionally, we show the ATR effectively intensified the co-precipitation process, potentially reducing plant size and cost, making it a suitable process for modular nuclear cleanup and post-management operations.

1. Introduction

As a result of the nuclear industry and other radioactive activities, large volumes of wastewater are produced containing dissolved radionuclides, which pose a potential threat to the public and the environment [1,2]. Radiocesium (^{137}Cs) and strontium (^{90}Sr) are two of the most important fission products with a half-life of about 30 years and emit penetrating beta and gamma radiation, which constitutes the main radioactivity in waste solutions [3]. Due to their high solubility and mobility in ecosystems, even low concentrations may lead to severe disease in humans [4–6]. Therefore, appropriate decontamination techniques are always required to separate and immobilise these radionuclides, especially given that larger volumes of effluent are expected to be generated from future decommissioning activities [7].

Treatment of radioactive waste is crucial to providing radiological protection and keeping nuclear power sustainable [2], and therefore, many studies have been undertaken on various separation techniques: ion exchange, adsorption, chemical precipitation, evaporation, membrane technologies, biological technologies, and their combined processes [6,8–20]. Of these, chemical precipitation is one of the more common traditionally used techniques to treat large volumes of concentrated radioactive wastewater, even in saline environments, thereby overcoming the coexisting ion effects [1,21–23]. However, precipitating agents for Cs^{+} ions are limited and inefficient at low concentrations due to the high solubility of cesium in water as well as experiencing difficulties in colloidal precipitate separation, thereby often requiring combined processes [1,13,24–26]. Comparatively, Sr^{2+} can be converted more easily into insoluble forms using carbonate and phosphate precipitants, but the formation of significant volumes of secondary wastes and solid-liquid separation difficulties are also critical issues [14,15]. In particular, barite ($BaSO_4$), known as an appropriate host mineral for capturing Sr^{2+}ions, can be used to allow efficient

* Corresponding authors.
E-mail addresses: pmoki@leeds.ac.uk (O. Kivan), t.n.hunter@leeds.ac.uk (T.N. Hunter).

https://doi.org/10.1016/j.cep.2024.110077
Received 21 August 2024; Received in revised form 2 November 2024; Accepted 18 November 2024
Available online 19 November 2024

co-precipitation of Sr^{2+} and rapid precipitate sedimentation arising from high density (4.48 g/cm^3) and exceptionally low solubility (K_{sp} $10^{-9.98}$) [27–30]. Furthermore, high resistance to radiation and desirable crystal stability to dissolution make $BaSO_4$ a superior host mineral for radioactive effluent treatment [27].

Alternatively, ion exchange/adsorption has also received attention in the treatment of radioactive effluents owing to its superior advantages such as simplicity, effectiveness, and minimal secondary waste formation [6,18,31–34]. In particular, clinoptilolite, a naturally occurring zeolite with the composition of (Na, K, Ca)$_2$–3Al$_3$ (Al, Si)$_2$Si$_{13}$O$_{36}$·12H$_2$O, is a widely studied crystalline aluminosilicate, exhibiting excellent ion exchange properties and radiation resistance. It is used to treat ^{137}Cs and ^{90}Sr ions in a number of nuclear sites, such as at the Site Ion Exchange Effluent Plant (SIXEP) in Sellafield, U.K, to decrease the concentration of radionuclides released to the Irish Sea [9, 35–37]. In addition, clinoptilolite is often used to reduce radiation hazards to the public from accidental nuclear releases, while it is considered a critical mineral for nuclear waste repositories, for example, in the Yucca Mountains case [38–40]. Its easy modification to increase the ion exchange capacity with appropriate treatment techniques and its ideal particle sizes for its versatile utilisation in both batch and column operations prove that it is a superior ion exchange material for radioactive effluent removal [9,11,41–43]. Nevertheless, clinoptilolite has a higher affinity for Cs^+ ions than Sr^{2+}, which is attributed to the suitable channel sizes of clinoptilolite (3.5–3.9 Å) to that of hydrated Cs^+ ions (3.45 Å) [41,44]. Moreover, unlike Cs^+ ions that tend to form inner-sphere complexes, Sr^{2+} shows lower adsorption affinity towards sorbent materials due to the formation of outer-sphere complexes [6]. Therefore, interest in the application of ion exchange/adsorption as a supporting step has increased to improve the removal efficiency of target pollutants, such as Sr^{2+}, especially with coagulation/flocculation systems [45,46].

Clinoptilolite can be utilised in both batch and column operations, where batch systems are known as more flexible, while the column units are the most used system in nuclear clean-up activities, e.g. SIXEP, as offering a more efficient process [41,43]. For example, a fixed bed column technique allows the purification of high effluent concentrations due to the continuous contact of contaminants with the adsorbent bed [42,47,48]. However, there are some drawbacks that affect column utilisation and removal efficiency; such as congestion, pressure loss, adsorbent replacement, cleaning, etc. [11,47]. Additionally, appropriate low flow rates and multiple columns are required to achieve better adsorption efficiency [32,42,47,49]. These factors negatively affect process footprints, operational cost, and throughput.

In terms of combined ion exchange and co-precipitation systems, incorporating fine ion exchange or adsorbents into a single combined adsorption-coagulation process may considerably improve overall process efficiency. In this case, as with pure co-precipitation, there will, however, be the need for a complex solid/liquid separation process and efficient sludge management and control [50]. In fact, the current authors utilised $BaSO_4$ for the enhanced coagulation with the aim of the simultaneous removal of Cs^+ and Sr^{2+} ions by combining with clinoptilolite ion exchange and showed that clinoptilolite-$BaSO_4$ composites improved both ion removal efficiency and dewaterability in all systems [51].

Generally, continuous stirred tank reactors (CSTRs) are perhaps the most widely used design for coagulation-based treatment owing to their simplicity and the agitation for perfect mixing in theory [50,52,53]. However, high energy consumption, space occupation, and the formation of heterogeneous precipitates in CSTRs increase the difficulties in treatment operations [50,54]. Thus, the concept of process intensification (PI) that primarily aims to reduce plant/equipment footprints while obtaining the desired performance has gained particular attention [55]. PI generally deals with innovative changes in process units through either novel designs or process combinations, ultimately resulting in step-changes in overall safety and efficiency in addition to providing smaller, cleaner, and sustainable operations [54–57]. Surprisingly, there have been few attempts to study PI in nuclear effluent treatment, where one of the most prominent examples was an investigation by Flouret et al. [58], who used a novel intensified reactor/classifier for Sr^{2+} removal in $BaSO_4$ coprecipitation. Alternatively, it is reported that an intensified plug-flow system is of superior benefit over CSTRs providing desirable process control and mass transfer in smaller reactor sizes, as well as waste reduction, since the lateral shear and mixing are independent of flow rates [52,54,59].

An example of an intensified design of a plug-flow reactor is the agitated tubular reactor (ATR) where an inner free-floating agitator bar generates lateral shear due to the mechanical moving of the reactor body, thereby separating mixing from the reactor flow [54,60,61]. As evident, the ATR can be utilised as a precipitator or ion exchange unit and even as a combined coagulation system due to its versatile design and effective separation units, and it has the potential for scaling up through up to ten additional reactor tubes [42,50,54,60,62]. Furthermore, the mixing behaviour of the ATR has shown that higher mass transfer is achieved compared to other mixing environments, such as batch reactors, owing to better energy dissipation originating from the lateral mixing [54,60]. This advantage may overcome the difficulties encountered in sorbent materials for simultaneously removing Cs^+ and Sr^{2+} ions caused by differences in electrostatic affinity and valence by improving adsorbent-ion contact and mixing [6,42]. So far, little attention has been paid to the performance of ATR type designs for nuclear effluent treatment, even if its desirable mixing behaviour evidences its potential for higher removal efficiencies and process intensification. Therefore, studying the performance of the ATR remains a need in the scope of process intensification in nuclear effluent treatment.

Herein, the main aims of this study were to compare the performance of a combined ion exchange-coagulation process using natural clinoptilolite and $BaSO_4$ in both batch and a process intensified system (ATR) for simultaneous removal of Cs^+ and Sr^{2+} ions. This study also set out to determine the physical characteristics of composite flocs synthesised in the batch and intensified systems to give an insight into the solid-liquid separation and difficulty of dewatering, assessed through the pressure filtration analyses. Furthermore, the influence of the shear rate in the ATR and the order of adding coagulating agents was investigated to understand the potential breakage of flocs and prevention of ion competition for optimal removal efficiency.

2. Materials and methods

2.1. Materials

Natural fine clinoptilolite powder was supplied from Holistic Valley Ltd with the reported approximate median size (d_{50}) of 10.5 μm. From the Electronic Supplementary Materials (ESM) Fig. S1, the measured particle size distribution gave a relatively broad distribution peak with the d_{50} ~10 μm, which is consistent with the manufacturer's size analysis and reported fine-milled clinoptilolite data [5,51]. Analytical grade cesium nitrate ($CsNO_3$) and strontium nitrate ($SrNO_3$) were obtained from Fluorochem Ltd. UK with purity ≥ 99 % and they were used as received. Barium chloride ($BaCl_2$) and sodium sulphate (Na_2SO_4) were of analytical grade, and also purchased from Fluorochem Ltd and utilised without purification. Ultrapure deionised Milli-Q™ water (Millipore, USA) was used to make solutions and for all dilution purposes throughout this study. Fluorescent tracer dye was used to study the plug flow behaviour of the ATR.

2.2. Batch adsorption and coagulation experiments

Batch-scale adsorption and coagulation experiments were conducted following a similar method to the one the current authors utilised in the previous study [51]. Initially, mixed Cs^+ and Sr^{2+} metal nitrate solutions were prepared by dilution from 1000 ppm stock solutions using to give

25 ppm of each metal ion in a total volume of 100 mL. Following mixing the solutions thoroughly, adsorption was performed by adding 4 g of the clinoptilolite powder to the metal solution to make the solid/liquid ratio 40 g/L, and the dispersion was then mixed on a magnetic stirrer plate at 300 rpm for 30 min. Coagulation was then initiated by dispersing 100 mL of 0.20 M $BaCl_2$ to make a reactive solution as described by Pacary et al. [63] (barium nitrate was used in that study). The reactive solution was mixed with the clinoptilolite-containing metal dispersion for 5 min and the composite flocs were then synthesised with $BaSO_4$ formation when 100 mL of 0.22 M Na_2SO_4 was mixed at 150 rpm for 10 min.

Additionally, samples of pure precipitated $BaSO_4$ were also produced to compare aggregate size and solid-liquid dewatering properties. A large litre scale of precipitation was carried out by introducing 500 mL of 0.22 M Na_2SO_4 solution into a 500 mL solution containing of 0.20 M $BaCl_2$, mixed at 150 rpm for 15 min.

Final coagulated suspension tubes were placed in a Heraeus Megafuge 16R (Thermo Scientific) for centrifugation for 10 min at 7000 rpm to separate the supernatants. These were filtered with 0.3 μm syringe filters for concentration analysis in a 240FS Atomic Absorption Spectrophotometer (AAS) (Varian-Agilent). The final concentrations of Cs^+ and Sr^{2+} were measured in AAS separately utilising different lamps for each ion according to different concentration ranges and wavelengths. Cesium concentration was analysed in absorbance mode using 852.1 nm wavelength for a 0.04–5 ppm working range, and the same instrument mode was also set for strontium using 460.7 nm wavelength for a 0.02–10 ppm working range. Additionally, 2 ppm and 5 ppm AAS standard solutions diluted from 1000 ppm standard stock (Thermo Scientific) were also used for instrument calibration for cesium and strontium, respectively. Notably, the combined batch study was repeated with a reverse additions of $BaCl_2$ and Na_2SO_4 solutions, denoted as reverse additions, to examine the differences in removal efficiency, due to expected Ba^{2+} competition for clinoptilolite adsorption sites [51].

Adsorption kinetics measurements were also conducted in 20 mL of mixed $CsNO_3$ and $SrNO_3$ metal solutions, giving 25 ppm of each ion. Here, the solid/liquid ratio was maintained at 20 g/L by dispersing 0.4 g of natural clinoptilolite, and all suspensions were mixed at 150 rpm for different kinetic times from 30 min to 24 h on an IKA® HS 260 (IKA Works, Inc., Germany) orbital shaker.

2.3. Coagulation in an agitated tubular reactor (ATR)

A pilot-scale Coflore® ATR (AM Technology, UK) was used to intensify the adsorption-coagulation process while aiming for a smaller plant footprint. The ATR can be operated with a series of connected reactor tubes where each contains a metal perforated agitator, allowing a plugflow mechanism by a high-rate radial shear when the reactor body is subjected to lateral oscillations (from 1 to 6 Hz) [60,62]. Improved mass transfer rates and regulated residence times make the ATR a suitable reactor design for adsorption-coagulation precipitations [54]. In this study, experiments were conducted in a separate test reactor mounted on top of the main ATR. It contained an approximately 392 mm long reactor with an inner tube diameter of 25.4 mm and 3 mm wall thickness, giving a total volume of ~150 mL [42,50]. The schematic illustration of the ATR test tube with its dimensions, along with a corresponding image that was taken during operation, are presented in Fig. 1. The residence time was maintained to that of batch experiment (~15 min) with regulated flow rates and concentration, calculated based on the reactor dimensions. In addition, two 520S peristaltic pumps (Watson-Marlow, Falmouth, UK) were utilised after calibration to prevent back pressure and to ensure that the flow rates were the same during the operation of the reactor.

The agitation frequency was set to 3 Hz and 5 Hz for each experiment to allow benchmarking of system efficiency along with the synthesised materials, since the sinusoidal motion of the ATR was reported to be optimal between 3 Hz and 5 Hz [61]. Prior to experiments, the plug-flow behaviour of the ATR was characterised by injecting 1000 ppm of dye solution into a fully water-filled reactor through the larger inlet for 1 min, with the flow rates the same as used in Tonge et al. with a similar system [50]. Water was then fed into the reactor via the same inlet to push the dye solution towards the outlet, diluting the dye solution throughout the residence time for observation. The dye analysis was performed at 3 Hz and 5 Hz agitation frequencies. The remaining dye concentration was then analysed utilising a Cary 60 UV–Vis

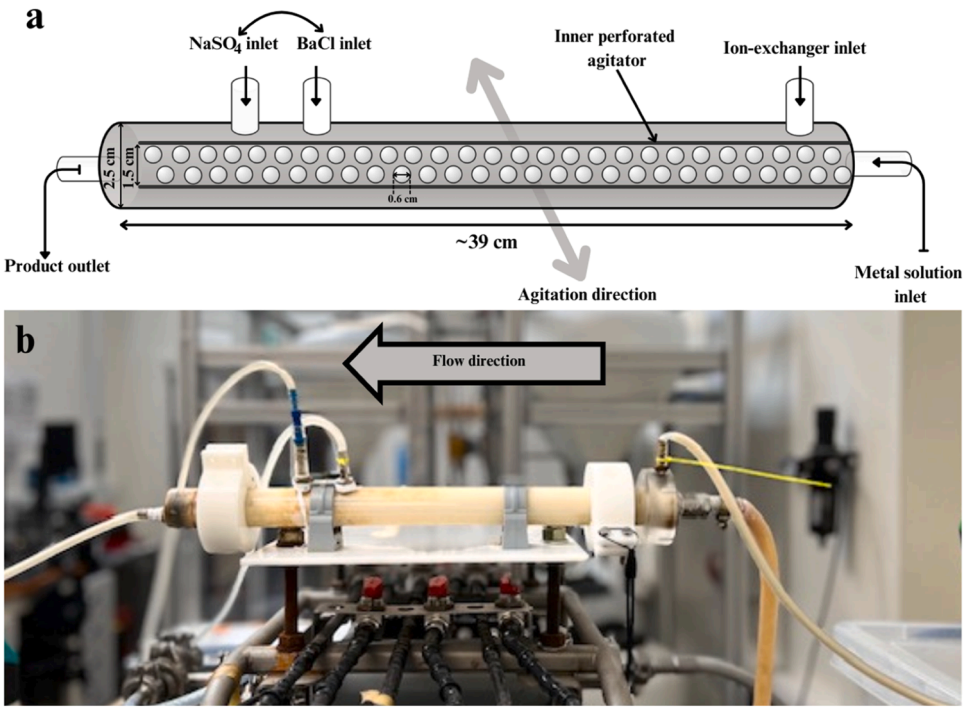

Fig. 1. Schematic representation of the ATR dimensions (a), and an image of the intensified combined adsorption-coagulation process during ATR operation (b).

spectrometer (Agilent Technologies) at wavelength spectrum from 200 nm to 800 nm.

For the combined adsorption and coagulation study, a 40 g/L clinoptilolite dispersion was prepared in 500 mL to give the same concentration as in the batch study, along with 1000 mL of mixed metal solution of Cs^+ and Sr^{2+} (containing 50 ppm of each ion), which was diluted down to 25 ppm when it mixed with clinoptilolite dispersion. Initially, the agitation frequency of the ATR was set up at 3 Hz and the mixed metal solution was injected into the ATR via the main inlet using a flow rate of ~ 11 ml/min. A low flow rate was used to maintain residence time similar to the batch system. Simultaneously, a secondary inlet was used to introduce the clinoptilolite dispersion at the same flow rate to allow equal mixing of both. As seen in Fig. 1, $BaCl_2$ and Na_2SO_4 solutions were separately injected via distinct inlets positioned beyond roughly two-thirds of the total length of the reactor (equivalent to ~10 mins residence time) and the synthesised composite clinoptilolite-$BaSO_4$ composites were collected from the outlet at ~15 min residence time. Thereafter, the same filtration procedure and AAS analysis were applied to the composite coagulants. The agitation frequency was increased to 5 Hz and the ATR was operated again for the combined system. Lastly, the ATR was operated to understand the effect of Ba^{2+} interference for clinoptilolite adsorption sites by modifying the injection order of the precipitate precursors. Here, Na_2SO_4 was injected in the first inlet and then $BaCl_2$ was introduced at the second reactor inlet.

2.4. Particle and aggregate characterisation

Particle characterisation of dried composite flocs was analysed in high-resolution scanning electron microscopy (SEM) (Hitachi SU8230) following 10 nm carbon coating with Q150TE evaporative coater (Quorum) to increase particle conductivity. Additionally, the penetration of Cs^+ and Sr^{2+} ions into clinoptilolite was investigated using Amber X focused plasma ions beam (FIB) SEM (TESCAN). Here, samples of clinoptilolite only were mixed with Cs^+ and Sr^{2+} metal solutions (following the procedure used for kinetics experiments) and mixed for 24 h. Dried powder samples were coated with 20 nm thick platinum to increase the resolution of a single grain of clinoptilolite. Scanning Transmission Electron Microscopy (STEM) analysis was performed with Titan^3 Themis 300 G2 (FEI, UK Ltd) under a 100 pA beam current at 300 kV for the elemental distribution of natural clinoptilolite used in this study. Before analysis, a drop of powdered natural clinoptilolite well dispersed in methanol was placed on a holey carbon-coated copper grid and the deeper regions of clinoptilolite were analysed to determine elemental distribution.

In addition, the Brunauer–Emmett–Teller (BET) surface area of natural clinoptilolite and synthesised composite coagulants were measured utilising a Tristar 3000 analyser (Micromeritics®, USA). Before measuring the N_2 adsorption/desorption isotherm, the samples were pretreated by heating at 200 °C for approximately 4 h under N_2 gas using FlowPrep™ 060 to degas the samples to remove moisture and impurities.

Aggregate particle size distributions were obtained from a Mastersizer 3000E (Malvern Panalytical Ltd) to determine how the agitation degree affects the size of the synthesised flocs in the ATR, thereby comparing it to composite flocs generated in the batch system. The settling rates of composite flocs under the Earth's gravitational force were analysed utilising a LUMiReader® X-Ray (L.U.M. GmbH) to understand to what degree the flocs create the fast settling beds without an external mechanical force, providing insight into sludge consolidation.

2.5. Pressure filtration

Pressure filtration analysis was studied to investigate the solid-liquid dewatering by applying pressure to the medium as a driving force [64]. The filtration analysis was performed in a batch filter utilising the HP4750 model high-pressure stirred filtration cell (Sterlitech™, USA) categorised as a dead-end filtration system. The HP4750 model consists of a stainless-steel cell that accommodates a 20 μm sized porous support membrane disc, allowing to process up to 300 ml with a maximum pressure of 69 bar (1000 psig). In this study, the filtration cell was filled with dispersions of the combined batch, ATR, and separately precipitated $BaSO_4$. Compressed air at 1, 2 and 3 bar, adjusted by a pressure regulator, was used to apply constant pressure to the filter cake from the top of the cell (1/4 FNPT tube).

The filtrates were then collected dropwise from a 0.125 cm diameter outlet tube and were weighted using an HR-250AZ analytical balance (A&D, Japan). A high-resolution camera setup was also used to record the exact filtrate. A schematic of the pressure filtration vessel and the analysis setup are shown in the Electronic Supplementary Materials (ESM) Fig. S2. Once the formed cake was consolidated, time over the filtrate volume (t/V) against filtrate volume was calculated using the measured mass. The gradient and the intercept from the linear trendlines were measured to calculate the specific cake resistance, α, and the medium resistance, R, respectively, by integrating them into the linear equation below rearranged from Darcy's law [65,66]:

$$\frac{t}{v} = \frac{\alpha \mu c}{2A^2 \Delta P} V + \frac{R_m \mu}{A \Delta P} \tag{1}$$

where t and v are the filtration time (s) and the volume of filtrate (m^3), respectively, c is the solid concentration per given volume (kg/m^3), μ is the viscosity of water, A is the area of the filtration (cm^2), ΔP is the driving pressure, and α and R_m are the constants for the specific cake resistance and the medium resistance, respectively, taken from the plot of t/V and V.

If the applied pressure is constant, the Eq. (1) is integrated and gives:

$$t = \frac{\alpha \mu c V^2}{2A^2 \Delta P} + \frac{R_m \mu V}{A \Delta P} \tag{2}$$

In this case, Eq. (2) can be interpreted to measure the specific cake resistance and the medium resistance from the gradient and intercept for as shown:

$$\frac{t}{V} = aV + b \tag{3}$$

As a result, the gradient (a) and the intercept (b) are then calculated in the form of equations:

$$a = \frac{\alpha \mu c}{2A^2 \Delta P} \tag{4}$$

and

$$b = \frac{R_m \mu}{A \Delta P} \tag{5}$$

Once the gradient and the intercept are taken from the t/V and V plot, the specific cake resistance (α) and the medium resistance (R_m) can be calculated utilising the Eq. (6) and Eq. (7) below:

$$\alpha = \frac{2A^2 \Delta P a(gradient)}{\mu c} \tag{6}$$

and

$$R_m = \frac{A \Delta P b(intercept)}{\mu} \tag{7}$$

Differences in pressure across the formed cake, known as pressure drop, play an important role in allowing fluid flow through the cake depending on its permeability which is inversely related to pressure drop, while pressure drop is of proportional relation to flow velocity according to Darcy's law [67]. The compressibility factor (n), also known as the scale-up constant, was also calculated using Eq. (8) below to study the behaviour of the specific cake resistance under applied constant pressure for the scalability of the filtration process:

$$\alpha_{av} = \alpha_0(\Delta P)^n \quad (8)$$

where α_{av} and ΔP are the experimental data for average specific cake resistance and the pressure drop through the cake (kPa), respectively; while α_0 and n stand for the specific cake resistance at zero pressure (m/kg) and the compressibility factor, respectively, taken from the logarithmic plot of α_{av} against ΔP [68,69]. It is noteworthy that the compressibility factor, n, is assessed between 0 and 1 for cakes, meaning the compressibility increases as the n is close to 1, and vice versa [68].

3. Results and discussion

3.1. Optimisation of ATR performance and materials characterisation

Fig. 2(a) presents images of the reactor taken during different operation times at 3 Hz agitation frequency during the dye tests. Here, it is clearly shown that the dye solution moves as a plug towards the reactor outlet (left of image) with water injected into the ATR tube. Qualitatively, it confirms minimum axial mixing was achieved throughout the ATR tube due to the ability to maintain radial mixing shear independent of reactor throughput [54].

Additionally, the plug-flow behaviour was examined by collecting dye samples from the reactor outlet every minute and analysing the dye concentration. Fig. 2(b) gives the residence time distribution showing the relative measured dye concentration (C/C_0) versus reactor operational times for 3 Hz frequency (red) and to 5 Hz (black) oscillation frequency. The narrow peak for 3 Hz indicates that a favourable plug-flow behaviour was achieved, owing to reduced axial dispersion with laminar flow, while 5 Hz agitation might have led to more axial dispersion and hence acted as more a pseudo plug-like flow system [70,71]. It is noted that the peak mean residence time occurred for both oscillations at ~13 min, rather than 15 min as initially assumed. The discrepancy was due to the volume of the agitator tube not being directly taken into account. Thus, the actual working reactor volume was slightly smaller than initially estimated.

Bianchi et al. [71] studied the flow characteristics of an oscillatory flow reactor and they stated that in the laminar flow system (with a low Reynold number), the axial mixing is limited with vortices formed by a higher degree of oscillation, which results in an ideal plug-flow system. However, they also added that axial dispersion may lead to a change plug-flow regime when the Reynold number reaches the critical level [71]. This may infer the fact that the plug-flow behaviour for 5 Hz agitation may have been changed due to increased axial dispersion with higher oscillation of the reactor body. Alternatively, Rice et al. [61] characterised the dynamics of ATR and stated that enhanced mixing and solids dispersion can be achieved with a 5 Hz agitation frequency due to the better sinusoidal motion of ATR.

Following the characterisation of the plug-flow behaviour, Cs^+/Sr^{2+} removal was studied using natural clinoptilolite only in the ATR, for direct comparison to batch performance. Fig. 3 presents the removal percentages of both ions in the ATR during different total continuous reactor operational times (all for a 13–15 min residence time), while clinoptilolite only batch adsorption kinetics and removal efficiencies can be found within the ESM (Fig. S3).

As observed, metals removal percent appears to reduce from close to 100% initially. This anomaly is because the reactor was initially filled with distilled water and the dilution of metal concentration at the inlet overestimated true removal efficiency. However, performance equilibrated after ~45 min (representing 3 reactor volumes being replaced) as more metal solution was injected into the ATR. Therefore, the

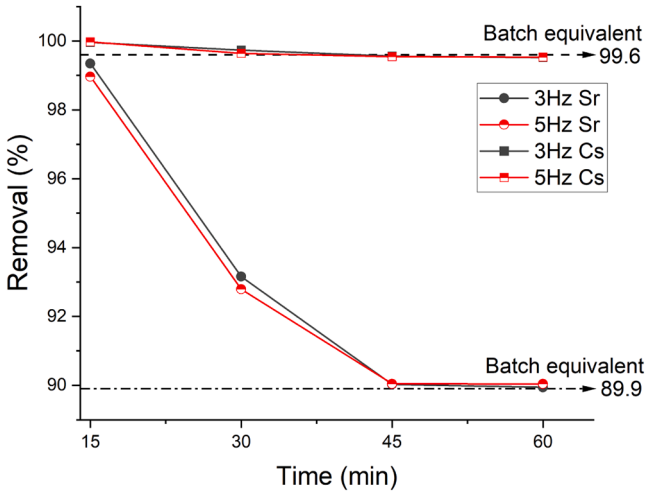

Fig. 3. Cs^+/Sr^{2+} removal using clinoptilolite in the ATR for different operational times. The dashed straight line indicates Cs^+ ions removal and the dot-dashed line represents Sr^{2+} ions removal at the equivalent residence time (15 min) from the batch adsorption study.

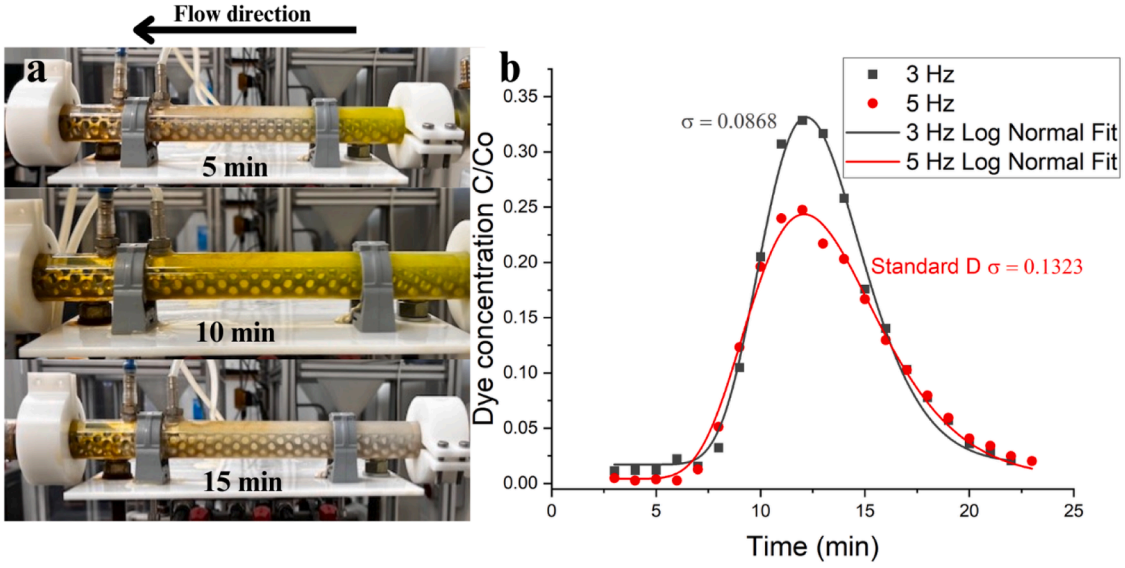

Fig. 2. Characterisation of plug-flow behaviour of ATR with a dye solution: (a) images taken during ATR operation at 3 Hz, (b) dye concentration versus time for 3 and 5 Hz agitation frequencies with standard deviations.

equilibrium performance for Sr^{2+} ion removal was ~ 90%, while a negligible decrease was seen for Cs^{+} removal maintained at around 99% for all reactor times.

Regarding the batch adsorption kinetics, Fig. S3 suggests that the kinetics reached the equilibrium within <1 h, while also giving significantly higher Cs^{+} removal (99.6%) than Sr^{2+} (89.9%) for the selected residence time (15 min). While the 15 min period was below the time to achieve equilibrium, significant adsorption was still achieved in this time. Given the requirement to process large effluent volumes for reduced footprint, a 15 min residence time was considered industrially optimised. Both batch and ATR data highlighted also the preferential adsorption of C^{s+} over Sr^{2+}. This performance differential of natural clinoptilolite is expected because of its higher cation selectivity for Cs^{+} compared to Sr^{2+} [72,73]. As given by the dashed horizontal lines in the Fig. 3, ATR showed slightly superior kinetic performance than the batch system for Cs^{+} ions, by providing a slightly higher Cs^{+} removal (99.97%) in the ATR than the batch reactor (99.60%) at the selected residence time. The equilibrium Sr^{2+} removal in the ATR was consistent with the batch reactor after 15 min. It is also noted that data at both 3 & 5 Hz presented effectively identical performance, indicating either frequency was able to fully disperse the clinoptilolite only with minimal issues.

From the ESM (Fig. S3), the Pseudo-Second Order (PSO) rate model showed a good relationship with the experimental adsorption data giving regression coefficients, $R^2 = 1$ for both ions, and hence the PSO rate model was applied to fit the adsorption kinetics, highlighting that chemical interactions via electrons exchange between clinoptilolite and Cs^{+}/Sr^{2+}play a key role in the rate-limiting step [74]. The PSO rate

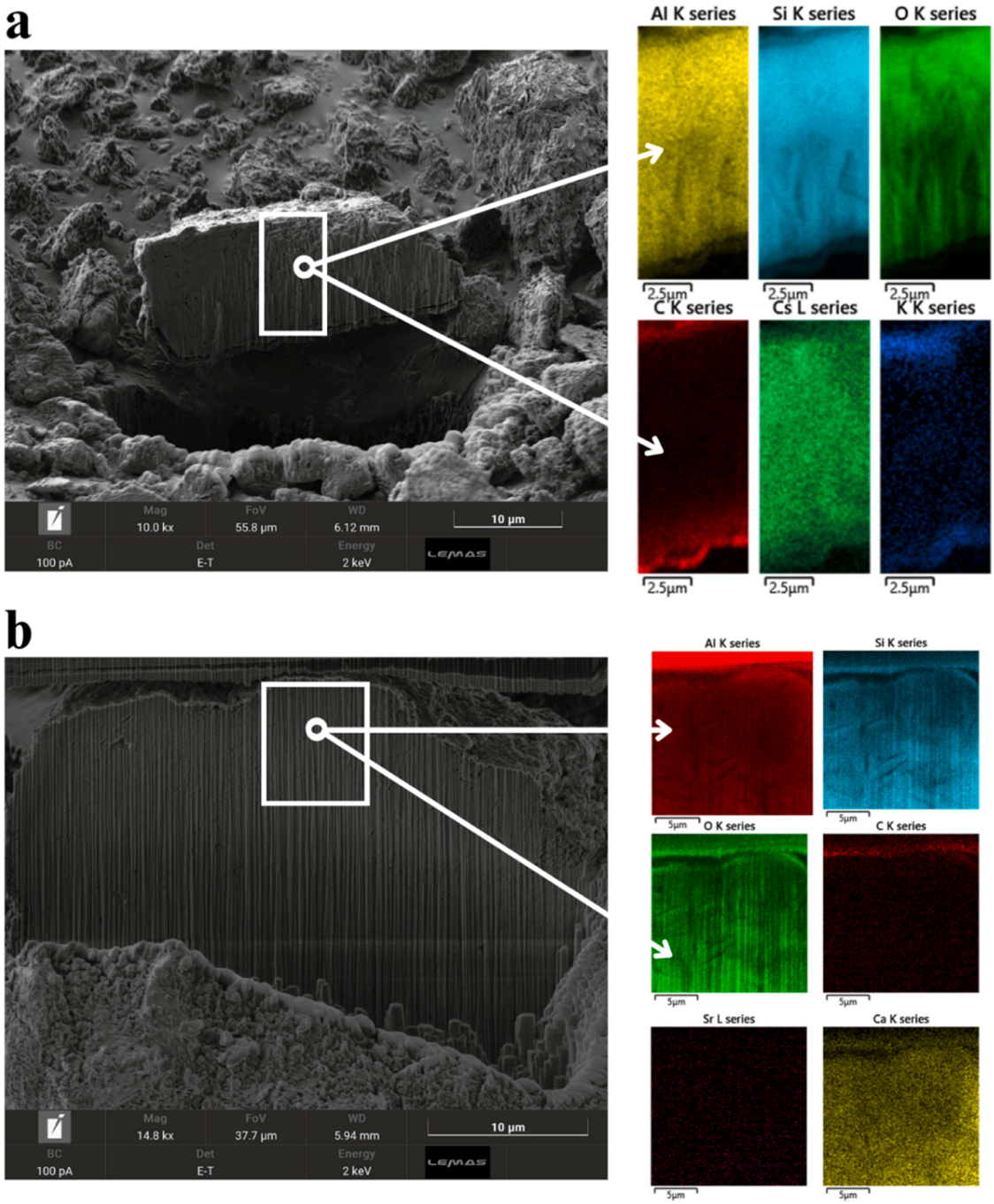

Fig. 4. FIB-SEM for 5000 ppm Cs^{+} (a) and Sr^{2+} (b) penetration through single grains of clinoptilolite, along with full EDS elemental maps.

model implies that surface chemisorption is the main mechanism in ion removal, driven by physicochemical interactions between the solid and liquid phases [11,75].

After ATR optimisation, FIB-SEM analysis was conducted on single crystals of clinoptilolite with a high 5000 ppm of Cs^+ and Sr^{2+} ion contamination, to determine the penetration depth of these ions within the clinoptilolite channel sites. In Fig. 4, the cut-through of clinoptilolite crystal doped with Cs^+ (a) and Sr^{2+} ions (b) is given with elemental distribution. Regarding other elements observed, carbon (used for conductive coating) is clearly seen only on the surface in both images, while Al, O, Si are throughout the crystal, as they are constituent elements of clinoptilolite. Interestingly, it is also clear that Cs^+ has penetrated deep into the clinoptilolite crystal and can be seen also within the entire cross-sectional area. This was not unexpected because the favourable channel structure and high Si/Al ratio of clinoptilolite may increase Cs^+ diffusion and hence penetrate through deeper clinoptilolite pores [76]. Noteworthy, Cs^+ density is lower in the regions where higher K^+ density is present and *vice versa*, which is evidence that K^+ is a competing ion for Cs^+ adsorption [11]. Regarding Sr^{2+} ions (Fig. 4, b) it is evident that Sr^{2+} does not penetrate nearly as much as Cs^+ ions, and only a small density can be seen within the clinoptilolite crystal lattice cross-section. The possible explanation could be the larger hydrated radius of Sr^{2+} (4.12 Å) than the size of hydrated Cs^+ (3.29 Å) and also the decrease in the charge density of the clinoptilolite framework due to less Al concentration that is favourable for higher removal and distribution of Cs^+ ions [72,77]. In addition, a higher density of Ca^{2+} ions present in the cross-sectional area may have led to a competitive effect on Sr^{2+} selectivity due to similar physicochemical properties [78].

As for the characterisation of natural clinoptilolite, TEM data for natural clinoptilolite used in this study is given within the ESM (Fig. S4), showing elemental distribution with competitive ions (such as K^+) and impurities. The BET surface area analysis of natural clinoptilolite and composite coagulants from the batch system was also carried out and N_2 adsorption/desorption isotherms are given within the ESM (Fig. S5). The recorded isotherm is classified as Type II based on the International Union of Pure and Applied Chemistry (IUPAC) adsorption isotherm classification, highlighting the macro-porosity of the clinoptilolite and the composite coagulants [79,80]. The surface area for clinoptilolite and composite coagulants was measured as 36.0 m^2/g and 18.3 m^2/g, respectively. The twofold reduction in composite coagulants may be the result of co-precipitation of clinoptilolite with $BaSO_4$, consistent with the $BaSO_4$ covering the surface of clinoptilolite while precipitating together.

The morphology of synthesised composite coagulants collected from the ATR, as well as from the batch reactor, was studied in a high-resolution SEM to determine the effects of the shear rates on the size and surface morphology of synthesised coagulants (Fig. 5). It is observed that the morphology of the fine clinoptilolite crystals is barely observed due to large clusters arising from the heterogeneous and almost spherical $BaSO_4$ crystals that were mostly located on the clinoptilolite surface while coagulating together. Consistent with the previous work by the current authors [51], analysis reviewed similar clusters, comprising clinoptilolite decorated by $BaSO_4$ crystals. With regards to agitation frequency, there were no major differences recorded between each agitation frequency in terms of the morphology, however, it appears that a larger number of smaller aggregates were present for samples at 5 Hz (Fig. 5b) compared to 3 Hz (Fig. 5c), noting the difficulty of deriving size information from dried SEM samples. It may be because the higher shear rate led to increased attritional breakdown of the composite coagulants , thereby distributing more uniformly [50].

3.2. Solid-liquid separation behaviour

Particle size distributions of the composite flocs collected from the ATR at different agitation frequencies, along with natural clinoptilolite, $BaSO_4$ and batch composite flocs are presented in Fig. 6(a) to validate the effect of different shear rates for flocs size. The particle size distribution of the composite flocs synthesised in the 3 Hz and 5 Hz ATR using reverse reagent additions is given within ESM (Fig. S6).

Monomodal distributions were observed for both 3 and 5 Hz composite flocs synthesised in the ATR, however, the mean sizes are noticeably smaller than for the batch produced composite flocs, although, less polydisperse than the $BaSO_4$ only precipitation. The oscillation frequency did also influence floc size to some degree, where under normal ATR conditions, the largest median size (d_{50}) was measured to be ~10.5 μm for flocs at 3 Hz agitation frequency, followed by flocs with a median size of ~8.15 μm from 5 Hz agitation. These differences are assumed due to the higher levels of shear within the ATR versus the magnetically stirred batch reactor. As evidenced in previous studies, shear rate plays a key role in enhanced mixing and facilitating flocculation, which is favourable for combined adsorption-coagulation analysis to remove ions, while it also inhibits larger aggregate formation by breaking them up when it reaches a sufficient rate to overcome particle forces [81–83]. Specifically, Tonge et al. [50] previously investigated the use of iron hydroxide precipitation to flocculate various mineral fines in an ATR, finding similarly, that the oscillating movement at 5 Hz reduced flocs with respects to a batch reactor. Nevertheless, it appears evident in the current findings that the use of a slower 3 Hz oscillation reduces this break-up, while there were also no operational issues with blockages to suggest poor solids dispersion at this lower rate. It is also noted that when the $BaCl_2$ and Na_2SO_4 additions were reversed, to reduce potential Ba^{2+} substitution with bound Cs^+ in the ion exchange, the final floc sizes were slightly smaller again (see ESM Fig. 6). It is thought that this may have been due to poorer attachment between the $BaSO_4$ precipitates and the clinoptilolite, as adsorbed Ba^{2+} ions also act as linkage sites to decorate the zeolite with the precipitates in a loose core-shell network [51].

The settling profiles over time for the composite coagulants taken from 3 Hz and 5 Hz agitation frequencies and from the batch study are given in Fig. 6(b), where the dashed lines indicate linear fitting for the initial zonal settling regions. Additionally, the final consolidated bed volume fractions and mean settling rates are given as an inset figure. As

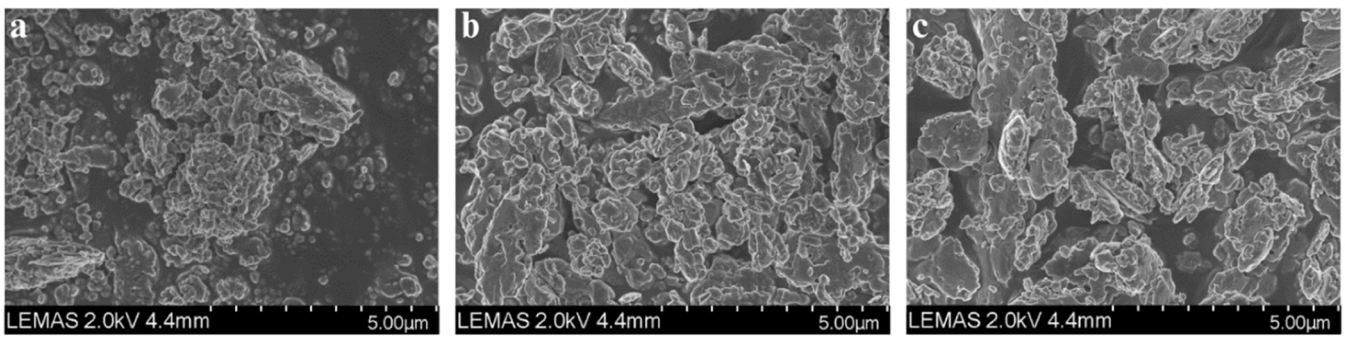

Fig. 5. Example scanning electron microscopy for composite coagulants from the batch reactor (a), and from the ATR at 5 Hz (b), and 3 Hz (c).

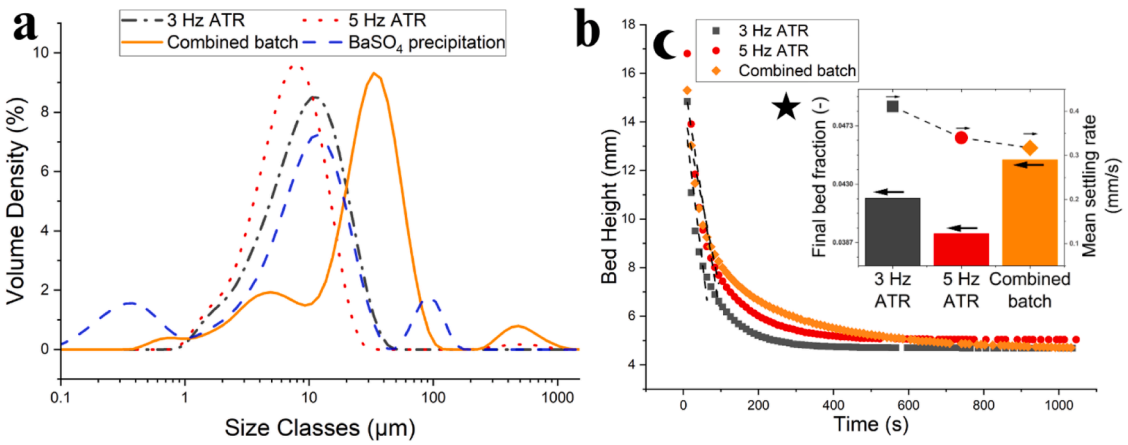

Fig. 6. (a) particle size distribution of composite flocs from ATR at 3 Hz (dot-dashed line) and 5 Hz (dotted line), $BaSO_4$ (dashed line) and composite flocs from combined batch (line), (b) X-ray settling rates (crescent symbol) of the combined batch, 3 Hz ATR agitation frequency, and 5 Hz agitation frequency. Dashed lines indicate the linear fitting of the settling area. Star inset, the final bed fraction and mean settling rate.

observed, all settling profiles exhibited similar sedimentation curves, however, there were some differences in initial settling rate. The fastest sedimentation was measured for 3 Hz agitation frequency, which settled in <100 s (at 0.4 mm/s). In comparison, slightly slower sedimentation was seen for flocs at 5 Hz agitation, at ~0.35 mm/s, and was slowest for the batch coagulation system, at ~0.33 mm/s. Final compressed volume fractions were similar in all three systems, although slightly greater for the batch system, and are consistent with previous gravity separated zeolite-$BaSO_4$ precipitates reported by the current authors [51].

What is most interesting about the sedimentation data, is that the rates for the ATR systems are greater than the batch flocculates, despite the fact that their aggregate sizes were markedly smaller (from Fig. 6 (a)). This would infer that, while smaller, the flocs from the ATR are substantially denser than produced in the batch reactor. It appears that the oscillatory shear may be low enough to allow continual re-structuring of the composite flocs, causing densification to the structure [81]. Importantly, this means that solid-liquid separation performance is similar for the ATR produced systems despite smaller aggregates size. Carissimi *et al.* [84] studied the settling rates of $Fe(OH)_3$ flocs in a mechanical agitator versus a plug flow system and found settling rates were ~ 4 times higher in the plug flow system (flocs generator reactor) than mechanical agitator, attributing to the better hydrodynamic environment for particles to form the flocs. The same research group also highlighted that the higher settling rates in the plug flow design led to short residence time and hence industrially smaller operational footprint as well as material savings [84]. Overall, it is evidence that the plug flow system of ATR improves the settling rates compared to the batch coagulation system and contributes to process intensification for a smaller operational footprint.

Furthermore, the settling rates of the reverse additions were also studied for 5 Hz agitation frequency and the combined batch, where the Na_2SO_4 was dispersed into the batch system before $BaCl_2$. Results given within the ESM (Fig. S7) clearly demonstrate that there are no major differences for 5 Hz agitation and the batch study in terms of settling behaviour when Ba^{2+} ions are injected later on, despite the floc sizes being smaller again (Fig. S6).

The filterability of synthesised suspensions was studied to assess the dewatering performance of the composite coagulants, in comparison to $BaSO_4$ only, by utilising a high-pressure filtration cell. In Fig. 7, the variation of specific cake resistance with different pressures (100, 200, 300 kPa, gauge) is given for pure precipitated $BaSO_4$ and composite flocs synthesised in both the batch system and the ATR (using 5 Hz oscillations). For the precipitated $BaSO_4$ only system, dispersions were made from dried power and set at 10 wt% (100 g/L) to ensure consistent baseline data. The dispersion concentrations for the combined batch and

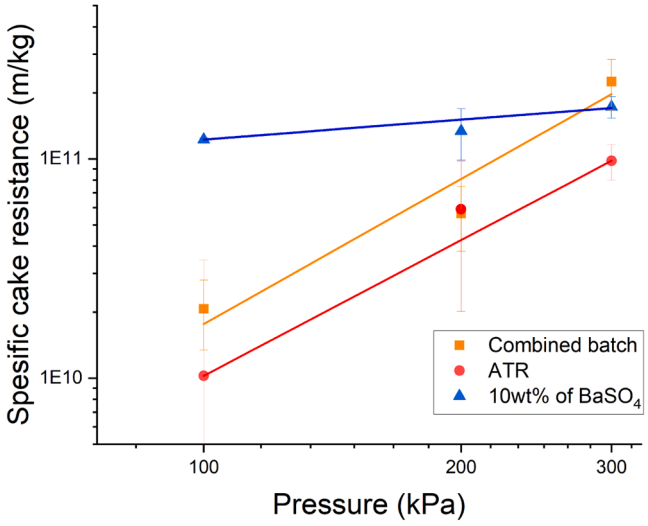

Fig. 7. Specific cake resistance under constant pressure for combined batch, 5 Hz ATR and 10 wt% $BaSO_4$ only precipitates.

ATR experiments were as per the synthesis conditions (~29 g/L). The raw t/V versus V data, used to calculate the specific cake and medium resistance (from the gradient and intercept respectively), are presented within the ESM (Fig. S8). Furthermore, the medium resistance (R_m) was also determined and is presented in the ESM (Table. S1). Generally, the R_m is stated to be constant during the filtration analysis [68]. However, there was some moderate variance was observed in the measured R_m values for some systems (see Table S1) which may be attributed to some loose finer particles filling pores on the medium at the start of the filtration upon initial consolidation, thus increasing the resistance [69].

As seen in Fig. 7, the specific cake resistance increased for all suspensions when the pressure was increased from 100 kPa to 300 kPa, as the particles may form a denser cake on the filter media, causing smaller pores and hence increased fritcional flow resistance [85]. Among the three systems, 10 wt% of precipitated $BaSO_4$ exhibited a significantly higher cake resistances than either of composite flocs at 100 kPa and 200 kPa applied pressure. It is assumed that this is due to the high specific flow resistance in the $BaSO_4$, because of the constituent nanocrystals that agglomerate on precipitation [51]. In the composite systems, as the $BaSO_4$ precipitates largely decorrelate the clinoptilolite, the specific surface area of the aggregates is thought to reduce, making dewatering less energy intensive. Indeed, the current authors also found that similar

composite flocs of the same materials achieved considerably greater volume fractions for equivalent compressive yield stresses than $BaSO_4$ only precipitates [51].

By contrast, it can be observed in Fig 7 that the composite flocs showed comparable compressibility than $BaSO_4$ precipitates at the highest applied pressure. At 100 kPa pressure, the combined batch system gave the cake resistance of 2.07×10^{10}, which increased markedly to 2.25×10^{11} when the pressure was increased to 300 kPa, and was in fact slightly greater than that of the 10 wt% $BaSO_4$ system. Because of the higher specific density of the composite flocs with respects to $BaSO_4$ only (either from the batch reactor or ATR) and their much greater compressibility, eventually network rearrangement of the filter cake at high pressures leads to increases to cake resistance to a point where it is no longer energetically feasible to perform the filtration. Indeed, in the prior compressive yield stress investigation by the current authors [51], while composite flocs were able to densify under compression much more so than $BaSO_4$ only flocs, final compressive yield stresses under high compression loads were also substantially higher. Therefore, there is evidence for greater network strength and increased resistance to dewatering at higher pressures, and thus for the composite flocs, low to moderate filter pressures are more favourable.

Interestingly also, the batch reactor composite flocs had consistently higher cake resistances than those from the ATR, at all pressures. It is assumed that this may be because of the greater density of the aggregates from the ATR (consistent with their high settling rates, despite their smaller sizes with respects to the batch reactor). It appears that the continual shearing and re-agglomeration of the clinoptilolite-flocs in the ATR from the oscillatory motion promotes more consistent flocs with lower specific resistance. It may also be from the greater size polydispersity evidenced from the batch reactor, where a small primary fines peak was evident (Fig. 6(a)) which could contribute to higher resistances through space filling in the pore networks.

Moreover, the compressibility factor (n) was calculated using Eq. (8) and presented within the ESM (Fig. S9). The compressibility factor was found to be 0.06 for 10 wt% of $BaSO_4$ precipitates, whereas the composite flocs synthesised in the batch and ATR system gave a greater compressibility factor of 0.427 and 0.539, respectively. $BaSO_4$ precipitates are therefore classified as a nearly incompressible cake because a compressibility factor of <0.2 indicates that the cake could show high resistance to compression [68]. This incompressibility of $BaSO_4$ may be due to the higher concentration of $BaSO_4$ precipitates that are initially above the gel point, thereby withstanding the consolidation [86]. On the other hand, the compressibility factor of composite flocs indicates highly compressible cakes. As discussed, it is possible that the different floc structures from the ATR system may have led to more porous cakes that were highly susceptible to compression. Park et al. [87] studied the cake properties of algae particles on a membrane system with different aluminium coagulant dosages, and they reported that the compressibility factor increased with larger dosages while giving lower specific cake resistance.

3.3. Cs^+/Sr^{2+} removal performance

The removal efficiencies of composite flocs synthesised in both batch and ATR systems for Cs^+ and Sr^{2+} ions are presented as in percentage in Fig 8(a) and Fig 8(b), respectively. The removal percentage of Sr^{2+} ions was higher in all systems compared to Cs^+ ions, which reflects the findings of the previous study by the current authors, due to some minor dissociation of Cs^+ with Ba^{2+} [51]. Regarding the combined batch study as given in orange bars, the composite flocs gave 99.92% removal efficiency for Sr^{2+} ions, whereas lower removal was achieved for Cs^+ ions giving 94.72% removal. These findings further support that $BaSO_4$ co-precipitation gives rise to enhanced Sr^{2+} removal because $BaSO_4$ crystals are an appropriate host mineral where Sr^{2+} ions are efficiently captured through different mechanisms, such as adsorption or incorporation due to having close ionic radii of Sr^{2+} to $BaSO_4$ crystal sites [27,

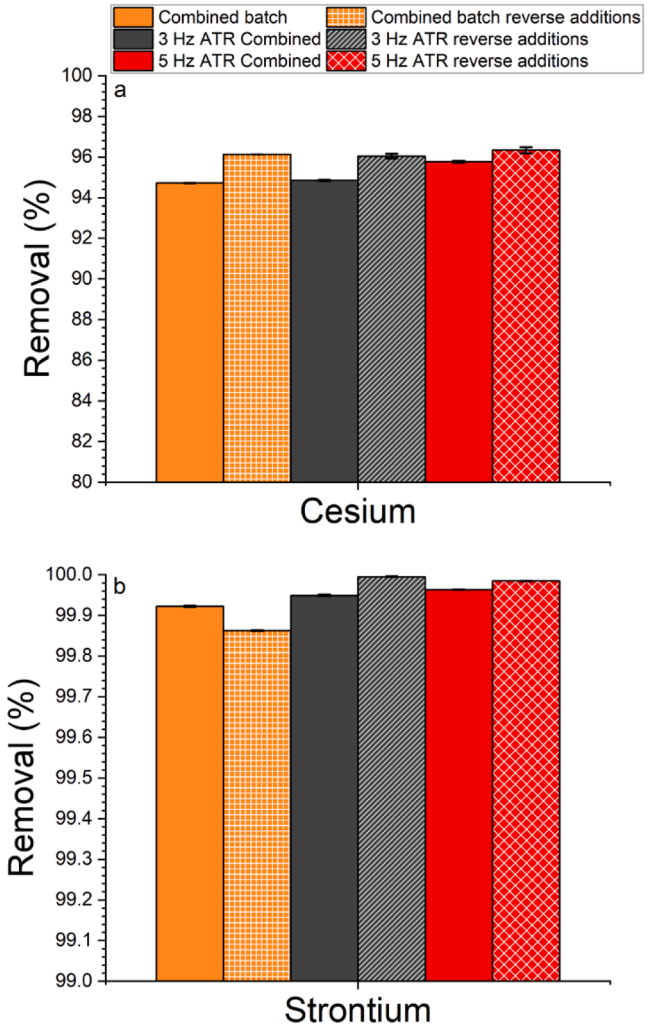

Fig. 8. The maximum removal percent of Cs^+ and Sr^{2+} ions in the batch, 3 & 5 Hz ATR and ATR with reverse addition systems; (a) Cs^+ removal, (b) Sr^{2+} removal in all systems.

51]. Comparatively, the natural clinoptilolite utilised in the present study showed equitable performance to material that was pre-activated with NaCl in the previous study using different clinoptilolite, highlighting the importance of geological properties on clinoptilolite cation exchange capacity [36,51]. Another possible explanation for this might be the lower iron and potassium contaminations in clinoptilolite used presently, as given in TEM data within the ESM (Fig. S4), possibly indicating reduced ion competition to the available clinoptilolite sites [11]. However, the reduction in Cs^+ removal efficiency in the combined batch study compared to the adsorption kinetics data should also be noted, as this is why the reverse additions of $BaCl_2$ and Na_2SO_4 was studied.

Therefore, to probe interference effect of Ba^{2+} ions on Cs^+ removal, the Na_2SO_4 solution was mixed first with the clinoptilolite suspension, before $BaCl_2$ addition in the batch reactor. The removal efficiency obtained from the batch reverse addition order can be compared in Fig. 8 (orange shaded bars). Interestingly, it is shown in Fig. 8(a) that Cs^+ removal was enhanced to 96.13% with a reverse addition of $BaCl_2$, suggesting that the competition effect of Ba^{2+} ions may be reduced in this way while giving more time for Cs^+ ions to interact with clinoptilolite adsorption sites. This result was not unexpected, as the ion selectivity of clinoptilolite was also reported to be relatively high for Ba^{2+} ions and, in fact, higher than for Sr^{2+} ions [44]. The further improvement for Sr^{2+} removal was not recorded with the reverse

addition order in the batch system, although, it still gave a favourable removal percentage of 99.86%.

As for the ATR data, it is apparent from Fig. 8 that the combined adsorption and coagulation process in the ATR outperformed the batch system in terms of the removal efficiency of both ions. As seen, the grey bar shows that Cs^+ removal was increased slightly to 94.84% at 3 Hz agitation, giving higher efficiency than the batch system, but lower than the batch reverse additions. The findings suggest that the Ba^{2+} ions may still compete with Cs^+ for clinoptilolite adsorption sites during ATR operation, even if an increase in removal efficiency was observed. In addition, Sr^{2+} removal was seen to be enhanced in the ATR when induced to 3 Hz agitation, giving a higher removal of 99.94% than both batch systems, which confirms that there is no Ba^{2+} ions effect on Sr^{2+} removal.

When the ATR was operated at a 5 Hz agitation frequency, a higher removal of 95.76% for Cs^+ ions was achieved again (Fig. 8 red bars) compared to the 3 Hz agitation. The same trend was also observed for Sr^{2+} removal, which gave a slight increase in efficiency to 99.96%. The further increase in ion removal in the ATR, especially for Cs^+, is assumed to be because of enhanced mixing and ideal solid dispersion obtained from a desirable sinusoidal motion of the inner ATR agitator when it is operated at 5 Hz agitation frequency [61]. Also, it seems possible that the increased agitation may result in a higher surface area to volume ratio due to synthesised smaller composite flocs, thereby increasing available adsorption sites for enhanced ion removal.

The reverse addition order of $BaCl_2$ and Na_2SO_4 was also studied in the ATR. From Fig. 8(a) (red shaded bars), it is observed that there is again a noticeable increase in Cs^+ removal with the injection of Na_2SO_4 prior to $BaCl_2$, giving 96.04% and 96.33% of Cs^+ removal when ATR was operated at 3 Hz and 5 Hz agitation frequency, respectively. Consistent with the reversed batch study, these results also support that the smaller residence time of $BaCl_2$ in the ATR, where injected through the inlet positioned closer to the reactor outlet, may cause less interaction of Ba^{2+} ions with clinoptilolite while giving more chance to Cs^+ ions to be adsorbed before the coagulation. Moreover, the superior sinusoidal motion obtained at 5 Hz agitation appears consistent with providing a higher Cs^+ removal efficiency than at 3 Hz agitation. Interestingly, as seen in Fig. 8(b), a further enhancement in Sr^{2+} removal was also recorded with the reverse additions, achieving >99.98% removal efficiencies for both frequency systems.

The superior performance of ATR compared to the batch system was assumed to be due to better mixing from favourable sinusoidal motions of ATR, as mentioned, as well as more efficient mass transfer resulting from higher energy dissipation than the batch system [60,61]. Tonge et al. [50] investigated dye removal with composite coagulants in a similar ATR and stated that the smaller residence time distributions and minimum side reactions due to high agitation degree may be other important factors for obtaining higher removal efficiency in ATR. Furthermore, Prajitno et al. [42] also operated an ATR to remove Cs^+ and Sr^{2+} ions using a clinoptilolite ion exchange column to compare its performance with a static column, finding that the ATR was able to treat three times the volume of water with 30% higher material performance compared to the static system [42]. Noteworthy, the ATR also provides approximately 1.5 times higher production rate than the batch system taking advantage of its equivalent reactor volume [50]. Industrially speaking, this result may also be evidence that the ATR fulfils the aims of the process intensification, by significantly reducing costs and operational footprint by utilising a smaller volume of ion exchange resins and coprecipitate reagents. Overall, ATR is an appropriate candidate for nuclear waste clean-up activities due to its modular design that can be easily scaled up with the operation of its 10 tubes simultaneously, while providing higher operational flexibility.

4. Conclusions

This study set out to benchmark the performance of composite flocs synthesised from natural clinoptilolite and (co)precipitation of $BaSO_4$ in both a batch reactor and an agitated tubular reactor (ATR) to separate Cs^+ and Sr^{2+} ions from the waste solution simultaneously. Furthermore, the sequence of $BaCl_2$ injection into the combined adsorption-coagulation process was also investigated for both systems to fully understand the effect of Ba^{2+} ions on Cs^+ removal efficiency.

The plug flow mechanism of ATR was initially studied using a fluorescent dye tracer at 3 Hz and 5 Hz agitation frequencies. The results suggested that a more ideal plug flow was achieved at 3 Hz agitation, where the axial vortices were reduced due to a low Reynold number. However, for an increased oscillation at 5 Hz agitation, secondary flows from the axial movement generated a more pseudo plug-flow behaviour with some broadening in the dye concentration peak. Metal ion removal tests in the ATR using clinoptilolite gave performance that was slightly better than in the batch reactor for a small 15 min residence time. For the combined composite flocs, the intensified combined adsorption-coagulation process led to an increase in Cs^+ and Sr^{2+} removal, giving the highest efficiency at 5 Hz agitation degree due to good sinusoidal motion of ATR where the mixing and solid dispersion were more enhanced. Critically, the highest removal percentages were achieved for both metals when the $BaCl_2$ was injected later than Na_2SO_4, giving >96% of Cs^+ and ~100% of Sr^{2+}. This result highlighted the possible interference effects of Ba^{2+} ions on Cs^+ removal.

Particle size, morphology and solid-liquid separation performance of the composite flocs were also studied to understand operational dewatering performance. Importantly, while the average particle sizes for flocs produced in the ATR were considerably smaller than from the batch reactor, they were also significantly denser, due to likely restructuring from the axial oscillations, resulting in enhanced sedimentation rates and compression. The filterability of dense composite flocs in comparison to pure precipitated $BaSO_4$ was also investigated in a high-pressure stirred filtration cell. The $BaSO_4$ gave specific cake resistances that were over an order of magnitude higher than the composite flocs for low to moderate pressures, due to their network structure of small nanosized crystallites. In comparison, the composite flocs presented greater compressibility as the pressure increased, resulting in a comparable cake resistance to $BaSO_4$ at the highest pressure tested. Thus, results suggest filtration at moderate pressures provide optimum dewatering.

Overall, the present study highlights that Cs^+ and Sr^{2+} ions can be separated simultaneously from the nuclear effluents by utilising composite coagulants. In addition, it allows the benchmarking of the performance of the ATR in terms of removal efficiency, emphasising a superior performance due to better mass transfer from the high energy dissipation. Furthermore, the ATR's modular design and ease of scale-up make it an appropriate candidate for nuclear clean-up operation, especially for Post Operational Clean Out (POCO) and unexpected large radioactive releases. Finally, this study also highlights an advantage of the composite precipitate flocs, in terms of their greater filterability and compressibility degree for radioactive sludge volume reduction and its better long-term storage.

CRediT authorship contribution statement

Oguzhan Kivan: Writing – review & editing, Writing – original draft, Visualization, Validation, Project administration, Methodology, Investigation, Funding acquisition, Formal analysis, Conceptualization. **Muhammad Yusuf:** Writing – review & editing, Validation, Supervision, Conceptualization. **Rachael Filson-Halliwell:** Writing – review & editing, Validation, Investigation. **Jennifer N. Enemmoh:** Writing – review & editing, Validation, Investigation. **David Harbottle:** Writing – review & editing, Supervision. **Timothy N. Hunter:** Writing – review & editing, Supervision, Resources, Project administration, Methodology, Funding acquisition, Conceptualization.

Declaration of competing interest

The authors declare the following financial interests/personal relationships which may be considered as potential competing interests:

Timothy N. Hunter reports financial support was provided by Engineering and Physical Sciences Research Council. If there are other authors, they declare that they have no known competing financial interests or personal relationships that could have appeared to influence the work reported in this paper.

Acknowledgements

Oguzhan Kivan gratefully thanks to the Republic of Türkiye Ministry of National Education for providing Ph.D. funding. The authors would also like to thank the Engineering and Physical Sciences Research Council (EPSRC) UK for funding and access to the x-ray sedimentation system, as part of the MULTIphase Fluid flOw in nucleaR systeMs (MULTIFORM) National Nuclear User Facility (grant: EP/V034898/1). The authors also would like to thank to Leeds Electron Microscopy and Spectroscopy Centre (LEMAS), Dr Ben Douglas, Christopher Bulman for their technical assistance.

Supplementary materials

Supplementary material associated with this article can be found, in the online version, at doi:10.1016/j.cep.2024.110077.

Data availability

The data of this study are openly available from the University of Leeds Data Repository at https://doi.org/10.5518/1565 [88].

References

[1] X. Zhang, P. Gu, Y. Liu, Decontamination of radioactive wastewater: state of the art and challenges forward, Chemosphere 215 (2019), https://doi.org/10.1016/j.chemosphere.2018.10.029.
[2] H. Ma, M. Shen, Y. Tong, X. Wang, Radioactive wastewater treatment technologies: a review, Molecules 28 (4) (2023), https://doi.org/10.3390/molecules28041935.
[3] A.M. James, S. Harding, T. Robshaw, N. Bramall, M.D. Ogden, R. Dawson, Selective environmental remediation of strontium and cesium using sulfonated hyper-cross-linked polymers (SHCPs), ACS Appl. Mater. Int. 11 (25) (2019), https://doi.org/10.1021/acsami.9b06295.
[4] Y.W. Chen, J.L. Wang, Removal of cesium from radioactive wastewater using magnetic chitosan beads cross-linked with glutaraldehyde, Nucl. Sci. Techn. 27 (2) (2016), https://doi.org/10.1007/s41365-016-0033-6.
[5] M.Y. Prajitno, S. Tangparitkul, H. Zhang, D. Harbottle, T.N. Hunter, The effect of cationic surfactants on improving natural clinoptilolite for the flotation of cesium, J. Hazard. Mater. 402 (2021), https://doi.org/10.1016/j.jhazmat.2020.123567.
[6] D. Alby, C. Charnay, M. Heran, B. Prelot, J. Zajac, Recent developments in nanostructured inorganic materials for sorption of cesium and strontium: synthesis and shaping, sorption capacity, mechanisms, and selectivity—a review, J. Hazard. Mater. 344 (2018), https://doi.org/10.1016/j.jhazmat.2017.10.047.
[7] T. Carey, C.D. Williams, D.J. McArthur, T. Malkinson, O.R. Thompson, A. Baidak, L. Murtagh, G. Glodan, S.P. Morgan, A.W. Banford, Removal of Cs, Sr, U and Pu species from simulated nuclear waste effluent using graphene oxide, J. Radioanal. Nucl. Chem. 317 (1) (2018), https://doi.org/10.1007/s10967-018-5931-0.
[8] I. Smičiklas, S. Dimović, I. Plećaš, Removal of Cs1+, Sr2+ and Co2+ from aqueous solutions by adsorption on natural clinoptilolite, Appl. Clay Sci. 35 (1) (2007), https://doi.org/10.1016/j.clay.2006.08.004.
[9] A. Dyer, J. Hriljac, N. Evans, I. Stokes, P. Rand, S. Kellet, R. Harjula, T. Moller, Z. Maher, R. Heatlie-Branson, J. Austin, S. Williamson-Owens, M. Higgins-Bos, K. Smith, L. O'Brien, N. Smith, N. Bryan, The use of columns of the zeolite clinoptilolite in the remediation of aqueous nuclear waste streams, J. Radioanal. Nucl. Chem. 318 (3) (2018), https://doi.org/10.1007/s10967-018-6329-8.
[10] X. Liu, J. Wang, Adsorptive removal of Sr2+ and Cs+ from aqueous solution by capacitive deionization, Environ. Sci. Pollut. R. 28 (3) (2021), https://doi.org/10.1007/s11356-020-10691-6.
[11] M.Y. Prajitno, D. Harbottle, N. Hondow, H. Zhang, T.N. Hunter, The effect of pre-activation and milling on improving natural clinoptilolite for ion exchange of cesium and strontium, J. Environ. Chem. Eng. 8 (1) (2020), https://doi.org/10.1016/j.jece.2019.102991.
[12] H. Zhang, Y.K. Kim, T.N. Hunter, A.P. Brown, J.W. Lee, D. Harbottle, Organically modified clay with potassium copper hexacyanoferrate for enhanced Cs+ adsorption capacity and selective recovery by flotation, J. Mater. Chem. A 5 (29) (2017), https://doi.org/10.1039/C7TA03873A.
[13] G.M. Rashad, M.R. Mahmoud, M.A. Soliman, Combination of coprecipitation and foam separation processes for rapid recovery and preconcentration of cesium radionuclides from water systems, Process. Saf. Environ. 130 (2019), https://doi.org/10.1016/j.psep.2019.08.007.
[14] J.G. Cao, P. Gu, J. Zhao, D. Zhang, Y. Deng, Removal of strontium from an aqueous solution using co-precipitation followed by microfiltration (CPMF), J. Radioanal. Nucl. Chem. 285 (3) (2010), https://doi.org/10.1007/s10967-010-0564-y.
[15] L.H.V. Thanh, J.C. Liu, Flotation separation of strontium via phosphate precipitation, Water Sci. Technol. 75 (11–12) (2017), https://doi.org/10.2166/wst.2017.129.
[16] A.A. Alsarayreh, T.K. Abbas, S.O. Alaswad, S. e-Gul, A.D. Bajoga, Remove liquid radioactive wastes utilizing nanofiltration, ultrafiltration, and microfiltration membranes, Eng. Technol. J. 40 (9) (2022), https://doi.org/10.30684/etj.2022.134025.1218.
[17] Y. Hu, X. Guo, C. Chen, J. Wang, Algal sorbent derived from Sargassum horneri for adsorption of cesium and strontium ions: equilibrium, kinetics, and mass transfer, Appl. Microbiol. Biotechnol. 103 (6) (2019), https://doi.org/10.1007/s00253-019-09619-z.
[18] S. Chen, J. Hu, S. Han, Y. Guo, N. Belzile, T. Deng, A review on emerging composite materials for cesium adsorption and environmental remediation on the latest decade, Sep. Purif. Technol. 251 (2020), https://doi.org/10.1016/j.seppur.2020.117340.
[19] S. Chen, J. Hu, J. Shi, M. Wang, Y. Guo, M. Li, J. Duo, T. Deng, Composite hydrogel particles encapsulated ammonium molybdophosphate for efficiently cesium selective removal and enrichment from wastewater, J. Hazard. Mater. 371 (2019), https://doi.org/10.1016/j.jhazmat.2019.03.047.
[20] M. Yusuf, D.S. Wisnubroto, The effect of saline water intrusion to cesium effluent processing, AIP Conf. Proc. 2967 (1) (2024), https://doi.org/10.1063/5.0192876.
[21] D. Fang, Y. Wang, H. Liu, H. Zhang, X. Ye, Q. Li, J. Li, Z. Wu, Efficient extraction of Rb+ and Cs+ by a precipitation flotation process with ammonium phosphowolframate as precipitant, Colloids Surf. A Physicochem. Eng. Asp. 608 (2021), https://doi.org/10.1016/j.colsurfa.2020.125581.
[22] R.O.A. Rahman, H.A. Ibrahium, Y.T. Hung, Liquid radioactive wastes treatment: a review, Water 3 (2) (2011), https://doi.org/10.3390/w3020551.
[23] S.G. Beheir, K. Benyamin, F.M. Mekhail, Chemical precipitation of cesium from waste solutions with iron(II)hexacyanocobaltate(III) and triphenylcyanoborate, J. Radioanal. Nucl. Chem. 232 (1) (1998), https://doi.org/10.1007/BF02383731.
[24] M.A. Soliman, G.M. Rashad, M.R. Mahmoud, Fast and efficient cesium removal from simulated radioactive liquid waste by an isotope dilution–precipitate flotation process, Chem. Eng. J. 275 (2015), https://doi.org/10.1016/j.cej.2015.03.136.
[25] J. Wang, S. Zhuang, Removal of cesium ions from aqueous solutions using various separation technologies, Rev. Environ. Sci. Bio. 18 (2) (2019), https://doi.org/10.1007/s11157-019-09499-9.
[26] K. Shakir, H.F. Ghoneimy, S.G. Beheir, M. Refaat, Flotation of cesium coprecipitated with nickel hexacyanoferrate(II) from aqueous solutions and radioactive waste simulants, Sep. Sci. Technol. 42 (6) (2007), https://doi.org/10.1080/01496390601174257.
[27] K. Tokunaga, N. Kozai, Y. Takahashi, A new technique for removing strontium from seawater by coprecipitation with barite, J. Hazard. Mater. 359 (2018), https://doi.org/10.1016/j.jhazmat.2018.07.044.
[28] M. Prieto, F. Heberling, R.M. Rodríguez-Galán, F. Brandt, Crystallization behavior of solid solutions from aqueous solutions: an environmental perspective, Prog. Cryst. Growth Character. Mater. 62 (3) (2016), https://doi.org/10.1016/j.pcrysgrow.2016.05.001.
[29] K. Tokunaga, Y. Takahashi, K. Tanaka, N. Kozai, Effective removal of iodate by coprecipitation with barite: behavior and mechanism, Chemosphere 266 (2021), https://doi.org/10.1016/j.chemosphere.2020.129104.
[30] H.A. Hunter, F.T. Ling, C.A. Peters, Metals coprecipitation with barite: nano-XRF observation of enhanced strontium incorporation, Environ. Eng. Sci. 37 (4) (2020), https://doi.org/10.1089/ees.2019.0447.
[31] M.A. Olatunji, M.U. Khandaker, H.N.M.E. Mahmud, Y.M. Amin, Influence of adsorption parameters on cesium uptake from aqueous solutions- a brief review, RSC Adv. 5 (88) (2015), https://doi.org/10.1039/C5RA10598F.
[32] A.M. El-Kamash, Evaluation of zeolite A for the sorptive removal of Cs+ and Sr2+ ions from aqueous solutions using batch and fixed bed column operations, J. Hazard. Mater. 151 (2) (2008), https://doi.org/10.1016/j.jhazmat.2007.06.009.
[33] B.R. Figueiredo, S.P. Cardoso, I. Portugal, J. Rocha, C.M. Silva, Inorganic ion exchangers for cesium removal from radioactive wastewater, Sep. Purif. Rev. 47 (4) (2018), https://doi.org/10.1080/15422119.2017.1392974.
[34] A. Ahmadpour, M. Zabihi, M. Tahmasbi, T.R. Bastami, Effect of adsorbents and chemical treatments on the removal of strontium from aqueous solutions, J. Hazard. Mater. 182 (1) (2010), https://doi.org/10.1016/j.jhazmat.2010.06.067.
[35] P. Rajec, K. Domianová, Cesium exchange reaction on natural and modified clinoptilolite zeolites, J. Radioanal. Nucl. Chem. 275 (3) (2008), https://doi.org/10.1007/s10967-007-7105-3.
[36] A.E. Osmanlioglu, Treatment of radioactive liquid waste by sorption on natural zeolite in Turkey, J. Hazard. Mater. 137 (1) (2006), https://doi.org/10.1016/j.jhazmat.2006.02.013.
[37] P. Sylvester, Strontium from nuclear wastes: ion exchange. 2000. p. 4261–4267.
[38] D.L. Bish, Natural zeolites and nuclear-waste management: the case of Yucca Mountain, Nevada, USA, in: P. Misaelides, F. Macášek, T.J. Pinnavaia, C. Colella (Eds.), Natural Microporous Materials in Environmental Technology, Dordrecht, Springer Netherlands, 1999, pp. 177–191.

[39] T. Armbruster, Clinoptilolite-heulandite: applications and basic research, Stud. Surf. Sci. Catal. 135 (2001), https://doi.org/10.1016/S0167-2991(01)81183-6.
[40] P. Misaelides, Application of natural zeolites in environmental remediation: a short review, Microporous Mesoporous Mater. 144 (1) (2011), https://doi.org/10.1016/j.micromeso.2011.03.024.
[41] R. Cortés-Martínez, M.T. Olguín, M. Solache-Ríos, Cesium sorption by clinoptilolite-rich tuffs in batch and fixed-bed systems, Desalination 258 (1) (2010), https://doi.org/10.1016/j.desal.2010.03.019.
[42] M.Y. Prajitno, M. Taufiqurrakhman, D. Harbottle, T.N. Hunter, Kinetic studies of Cs + and Sr2+ ion exchange using clinoptilolite in static columns and an Agitated Tubular Reactor (ATR), ChemEngineering 5 (1) (2021), https://doi.org/10.3390/chemengineering5010009.
[43] International, Atomic, Energy, Agency, Application of Ion Exchange Processes for the Treatment of Radioactive Waste and Management of Spent Ion Exchangers, IAEA, Vienna, 2002.
[44] M. Dosa, M. Piumetti, S. Bensaid, N. Russo, O. Baglieri, F. Miglietta, D. Fino, Properties of the clinoptilolite: characterization and adsorption tests with methylene blue, J. Adv. Catal. Sci. Techno. (2018), https://doi.org/10.15379/2408-9834.2018.05.01.01.
[45] S. Papić, N. Koprivanac, A. Lončarić Božić, A. Meteš, Removal of some reactive dyes from synthetic wastewater by combined Al(III) coagulation/carbon adsorption process, Dyes Pigm. 62 (3) (2004), https://doi.org/10.1016/S0143-7208(03)00148-7.
[46] J.W. Lee, S.P. Choi, R. Thiruvenkatachari, W.G. Shim, H. Moon, Evaluation of the performance of adsorption and coagulation processes for the maximum removal of reactive dyes, Dyes Pigm. 69 (3) (2006), https://doi.org/10.1016/j.dyepig.2005.03.008.
[47] H. Patel, Fixed-bed column adsorption study: a comprehensive review, Appl. Water Sci. 9 (3) (2019), https://doi.org/10.1007/s13201-019-0927-7.
[48] M. Kebir, H. Tahraoui, M. Chabani, M. Trari, N. Noureddine, A.A. Assadi, A. Amrane, N. Ben Hamadi, L. Khezami, Water cleaning by a continuous fixed-bed column for Cr(VI) eco-adsorption with green adsorbent-based biomass: an experimental modeling study, Processes 11 (2) (2023), https://doi.org/10.3390/pr11020363.
[49] A. Ararem, O. Bouras, A. Bouzidi, Batch and continuous fixed-bed column adsorption of Cs+ and Sr2+ onto montmorillonite–iron oxide composite: comparative and competitive study, J. Radioanal. Nucl. Chem. 298 (1) (2013), https://doi.org/10.1007/s10967-013-2433-y.
[50] A.S. Tonge, D. Harbottle, S. Casarin, M. Zervaki, C. Careme, T.N. Hunter, Coagulated mineral adsorbents for dye removal, and their process intensification using an Agitated Tubular Reactor (ATR), ChemEngineering 5 (3) (2021), https://doi.org/10.3390/chemengineering5030035.
[51] O. Kivan, M. Yusuf, D. Harbottle, T.N. Hunter, Removal of cesium and strontium ions with enhanced solid-liquid separation by combined ion exchange and BaSO4 co-precipitation, J. Water Process. Eng. 59 (2024), https://doi.org/10.1016/j.jwpe.2024.104934.
[52] Chapter 5 - Reactors, in: D. Reay, C. Ramshaw, A. Harvey (Eds.), Process Intensification, Oxford, Butterworth-Heinemann, 2008, pp. 103–186.
[53] V. Pacary, Y. Barré, E. Plasari, Modeling and comparison of continuous and semi-continuous processes for simulating decontamination of liquid nuclear wastes by the coprecipitation of strontium ions with barium sulphate, Int. J. Chem. React. Eng. 6 (1) (2008), https://doi.org/10.2202/1542-6580.1643.
[54] G. Yaghy, A.S. Tonge, H. Abouhakim, R. Peeling, M. Talford, L. O'Brien, A. Paksy, P. Nevitt, F.L. Muller, B.C. Hanson, T.N. Hunter, Opportunities for process intensification technologies in nuclear effluent treatment: a review of precipitators, adsorbers and separators, Chem. Eng. Process. 191 (2023), https://doi.org/10.1016/j.cep.2023.109441.
[55] A.I. Stankiewicz, J.A. Moulijn, Process intensification: transforming chemical engineering, Chem. Eng. Prog. 96 (1) (2000).
[56] C. Tsouris, J.V. Porcelli, Process intensification - has its time finally come? Chem. Eng. Prog. 99 (2003).
[57] M. Baldea, From process integration to process intensification, Comput. Chem. Eng. 81 (2015), https://doi.org/10.1016/j.compchemeng.2015.03.011.
[58] J. Flouret, Y. Barré, H. Muhr, E. Plasari, Design of an intensified coprecipitation reactor for the treatment of liquid radioactive wastes, Chem. Eng. Sci. 77 (2012), https://doi.org/10.1016/j.ces.2012.01.051.
[59] M. Avila, B. Kawas, D.F. Fletcher, M. Poux, C. Xuereb, J. Aubin, Design, performance characterization and applications of continuous oscillatory baffled reactors, Chem. Eng. Process. 180 (2022), https://doi.org/10.1016/j.cep.2021.108718.
[60] Y. He, A.E. Bayly, A. Hassanpour, M. Fairweather, F. Muller, Flow behaviour of an agitated tubular reactor using a novel dynamic mesh based CFD model, Chem. Eng. Sci. 212 (2020), https://doi.org/10.1016/j.ces.2019.115333.
[61] H.P. Rice, Y. He, F.L. Muller, A.E. Bayly, R. Ashe, A. Karras, A. Hassanpour, R. A. Bourne, M. Fairweather, T.N. Hunter, Physical and numerical characterisation of an agitated tubular reactor (ATR) for intensification of chemical processes, Chem. Eng. Process. 179 (2022), https://doi.org/10.1016/j.cep.2022.109067.
[62] J. Miller, B. Hanson, F. Muller, Design Optimisation for Solvent Extraction in a Modified Agitated Tube Reactor - 19400, United States, 2019.
[63] V. Pacary, Y. Barré, E. Plasari, Method for the prediction of nuclear waste solution decontamination by coprecipitation of strontium ions with barium sulphate using the experimental data obtained in non-radioactive environment, Chem. Eng. Res. Des. 88 (9) (2010), https://doi.org/10.1016/j.cherd.2010.01.006.
[64] E. Höfgen, S. Kühne, U.A. Peuker, A.D. Stickland, A comparison of filtration characterisation devices for compressible suspensions using conventional filtration theory and compressional rheology, Powder Technol. 346 (2019), https://doi.org/10.1016/j.powtec.2019.01.056.
[65] Y. Li, Y. Chen, W. Xia, G. Xie, Filtration of kaolinite and coal mixture suspension: settling behavior and filter cake structure analysis, Powder Technol. 381 (2021), https://doi.org/10.1016/j.powtec.2020.12.050.
[66] L. Svarovsky, 9 - Filtration fundamentals, in: L. Svarovsky (Ed.), Solid-Liquid Separation (Fourth Edition), Oxford, Butterworth-Heinemann, 2001, pp. 302–334.
[67] A. De Haan, H. Bosch, Industrial Separation Processes - Fundamentals, De Gruyter, Berlin, Boston, 2013.
[68] S. Tarleton, R. Wakeman, Solid/Liquid Separation: Principles of Industrial Filtration, Elsevier Science, 2005.
[69] F.M. Mahdi, R.G. Holdich, Laboratory cake filtration testing using constant rate, Chem. Eng. Res. Des. 91 (6) (2013), https://doi.org/10.1016/j.cherd.2012.11.012.
[70] D.Y. Sheng, Z. Zou, Application of tanks-in-series model to characterize non-ideal flow regimes in continuous casting Tundish, Metals 11 (2) (2021).
[71] P. Bianchi, J.D. Williams, C.O. Kappe, Oscillatory flow reactors for synthetic chemistry applications, J. Flow Chem. 10 (3) (2020), https://doi.org/10.1007/s41981-020-00105-6.
[72] S. Fan, L. Jiang, Z. Jia, Y. Yang, L.a. Hou, Comparison of adsorbents for cesium and strontium in different solutions, Separations 10 (4) (2023), https://doi.org/10.3390/separations10040266.
[73] F.A. Mumpton, La roca magica: uses of natural zeolites in agriculture and industry, Proc. Natl. Acad. Sci. U.S.A. 96 (7) (1999), https://doi.org/10.1073/pnas.96.7.3463.
[74] Y.S. Ho, G. McKay, Pseudo-second order model for sorption processes, Process Biochem. 34 (5) (1999), https://doi.org/10.1016/S0032-9592(98)00112-5.
[75] D.A. De Haro-Del Rio, S. Al-Joubori, O. Kontogiannis, D. Papadatos-Gigantes, O. Ajayi, C. Li, S.M. Holmes, The removal of caesium ions using supported clinoptilolite, J. Hazard. Mater. 289 (2015), https://doi.org/10.1016/j.jhazmat.2015.02.032.
[76] E. Duque-Redondo, K. Yamada, E. Masoero, J.Bañuelos Prieto, H. Manzano, Adsorption and migration of Cs and Na ions in geopolymers and zeolites, Mater. Today Commun. 36 (2023), https://doi.org/10.1016/j.mtcomm.2023.106496.
[77] S. Kwon, C. Kim, E. Han, H. Lee, H.S. Cho, M. Choi, Relationship between zeolite structure and capture capability for radioactive cesium and strontium, J. Hazard. Mater. 408 (2021), https://doi.org/10.1016/j.jhazmat.2020.124419.
[78] S. İnan, Inorganic ion exchangers for strontium removal from radioactive waste: a review, J. Radioanal. Nucl. Chem. 331 (3) (2022), https://doi.org/10.1007/s10967-022-08206-3.
[79] M. Thommes, K. Kaneko, A.V. Neimark, J.P. Olivier, F. Rodriguez-Reinoso, J. Rouquerol, K.S.W. Sing, Physisorption of gases, with special reference to the evaluation of surface area and pore size distribution (IUPAC Technical Report), Pure Appl. Chem. 87 (9–10) (2015), https://doi.org/10.1515/pac-2014-1117.
[80] Z.A. ALOthman, A review: fundamental aspects of silicate mesoporous materials, Materials 5 (12) (2012), https://doi.org/10.3390/ma5122874.
[81] W.S. Ng, L.A. Connal, E. Forbes, K. Mohanarangam, G.V. Franks, In situ investigation of aggregate sizes formed using thermo-responsive polymers: effect of temperature and shear, J. Colloid Interface Sci. 494 (2017), https://doi.org/10.1016/j.jcis.2017.01.067.
[82] G.V. Franks, P.D. Yates, N.W.A. Lambert, G.J. Jameson, Aggregate size and density after shearing, implications for dewatering fine tailings with hydrocyclones, Int. J. Miner. Process. 77 (1) (2005), https://doi.org/10.1016/j.minpro.2005.02.002.
[83] M. Pieper, S. Aman, J. Tomas, Agglomeration kinetics of submicron barium sulfate precipitates, Chem. Eng. Sci. 77 (2012), https://doi.org/10.1016/j.ces.2011.12.043.
[84] E. Carissimi, J.D. Miller, J. Rubio, Characterization of the high kinetic energy dissipation of the Flocs Generator Reactor (FGR), Int. J. Miner. Process. 85 (1) (2007), https://doi.org/10.1016/j.minpro.2007.08.001.
[85] D. Antelmi, B. Cabane, M. Meireles, P. Aimar, Cake collapse in pressure filtration, Langmuir 17 (22) (2001), https://doi.org/10.1021/la0104471.
[86] A.D. Stickland, C. Burgess, D.R. Dixon, P.J. Harbour, P.J. Scales, L.J. Studer, S. P. Usher, Fundamental dewatering properties of wastewater treatment sludges from filtration and sedimentation testing, Chem. Eng. Sci. 63 (21) (2008), https://doi.org/10.1016/j.ces.2008.07.016.
[87] K. Park, P. Kim, H.G. Kim, J. Kim, Membrane fouling mechanisms in combined microfiltration-coagulation of Algal rich water applying ceramic membranes, Membranes 9 (2) (2019), https://doi.org/10.3390/membranes9020033.
[88] O. Kivan, M. Yusuf, R. Filson-Halliwell, J.N. Enemmoh, D. Harbottle, T.N. Hunter, Intensified co-precipitation and ion exchange using an agitated tubular reactor (ATR) for enhanced removal of Cs+ and Sr2+ ions. 2024.